Journal of Sound and Vibration (2001) **243**(3), 381–401
doi:10.1006/jsvi.2000.3411, available online at http://www.idealibrary.com on IDEAL®

ACOUSTIC PROPAGATION IN DUCTS WITH SLOWLY VARYING ELLIPTIC CROSS-SECTION

N. Peake and A. J. Cooper

Department of Applied Mathematics and Theoretical Physics, University of Cambridge, Silver Street, Cambridge CB3 9EW, England. E-mail: n.peake@damtp.cam.ac.uk

(*Received* 22 *February* 2000, *and in final form* 9 *August* 2000)

The propagation of acoustic waves along a duct of elliptic cross-section, the eccentricity of which varies slowly along the axis, is considered as a model of the unsteady flow inside a realistic aeroengine nacelle. This is a development of recent work on a circular duct by Rienstra. The acoustic field at each axial location is expanded in terms of the local even and odd Mathieu modes, and the slow variation of the axial wavenumber and the modal amplitude along the duct are determined as part of the solution. The duct eccentricity is seen to have a very significant effect right across the range of practical azimuthal orders, and has different effects on the even and odd modes. For instance, the point at which a given mode changes from being cut-on to cut-off depends on the eccentricity; for even modes, and for the odd modes apart from at a very low frequency, the eccentricity makes modes more cut-on than in a circular duct. Even for cases in which a given mode is cut-on all along the duct according to standard circular duct theory, the modal amplitude is seen to depend strongly on the cross-sectional eccentricity. In a representative case the amplitude of a high order mode propagating upstream along a slowly varying elliptical duct is seen to be significantly lower than that of the equivalent mode propagating in a circular duct of the same cross-sectional area.

© 2001 Academic Press

1. INTRODUCTION

The understanding of the way in which acoustic waves propagate along the nacelle is a central feature of the prediction of the noise generated by aeroengines. Classical analysis has typically assumed that the duct has a circular cross-section which is uniform along its axis, leading to a model structure involving Bessel functions—see for instance reference [1]. However, on very large aeroengines the intakes are not axisymmetric, because ground clearance requirements mean that the nacelle is often "squashed" in the vertical direction. Moreover, the cross-section will vary along the axis, being typically circular at the fan face but becoming non-axisymmetric further upstream. There is therefore a practical need to predict the effects of nacelle asymmetry and axial variation on the sound inside the nacelle, and the aim of this paper is to complete the analysis of a realistic model problem which includes both these features. Specifically, a duct with (for definiteness) elliptic cross-section, the eccentricity of which varies along the axis, is considered.

There has been considerable early interest in the acoustics of elliptic jets—see, for example, references [2–4]. This analysis essentially involves solution of the Helmholtz equation (or of a modified equation to account for non-uniform axial flow) in elliptic co-ordinates, which in turn is completed by these authors in terms of Mathieu functions [5]. Exactly the same style of analysis will be used in the present elliptic duct problem. On the other hand, the problem of a circular duct with slow axial variation in its radius has been

0022-460X/01/230381 + 21 $35.00/0 © 2001 Academic Press

considered by Nayfeh and others [6, 7], but recently a fully analytical solution has been derived by Rienstra [8] using the multiple-scales technique—see reference [9]. Specifically, a slow axial scale $X = \varepsilon x$ is introduced, where $\varepsilon \ll 1$ and x is the conventional axial co-ordinate. The small parameter ε can be defined to be, for instance, the mean gradient of the outer nacelle wall in the axial direction. This approximation of relatively slow variation in nacelle geometry along the axis is a good one in practice—see reference [10] for an impressive comparison between the asymptotics and a fully numerical solution. In this paper, we therefore propose to unify these two different strands of work by considering a slowly varying duct with *elliptic* cross-section. For practical relevance, we insist that the duct carries a (subsonic) steady flow, which must necessarily itself vary along the axis due to the shape changes and which must be found as a part of our solution.

Duct mode propagation is crucial to at least two areas of aeroengine behaviour. First, it is related to the farfield noise; radiation from the fan propagates upstream in the form of duct modes, and is then radiated from the open end of the duct—see references [11, 12]. The azimuthal order, m, of the duct modes which radiate is typically rather large, and depends on the number of blades in the fan, so that m would be expected to be in the range 20–30. Second, duct-mode propagation is related to fan instability; it has recently been shown [13] that acoustic modes can be trapped by area variations ahead of the fan and swirl behind the fan, leading to possible fan excitation, and these instabilities tend to occur for low azimuthal orders, typically $m \leqslant 6$. In order to demonstrate the possible relevance of the effects of an elliptic intake on both the noise and the mode trapping, the results for a wide range of azimuthal orders will therefore be presented.

In order to fit the duct geometry a modified elliptic–cylindrical co-ordinate system is used, in which the eccentricity varies along the axis. Since this is a non-orthogonal system, some care must be taken in deriving the various differential operators. This is described in section 2, together with the governing equations. In section 3, the solution of these equations is described, very much along the lines set out by Rienstra [8] for the circular duct. First, the steady flow is determined, which in the asymptotic limit considered here is governed by one-dimensional gas dynamics. Second, the $O(1)$ approximation to the unsteady flow is determined, which provides the local modal structure of the acoustic field in terms of Mathieu functions—unlike the circular case, there are now two quite distinct families of modes, one even about the ellipse semi-major axis and the other odd. The variation in the axial wavenumber along the duct is also provided at this order, showing at what points (if any) the modes can change from propagating (cut-on) to evanescent (cut-off). Finally, the $O(\varepsilon)$ correction to the unsteady flow is considered, which provides a secularity condition to determine the variation of the leading order modal amplitudes. In section 4, results for a realistic intake are presented, for both the cut-on/cut-off behaviour of the modes and the variation in amplitudes along the duct, and it is seen that both are significantly affected by the duct asymmetry. It can therefore be concluded that classical circular duct theory must be inapplicable in a range of important practical situations.

2. PROBLEM FORMULATION

2.1. GEOMETRY

Consider a straight duct with axis aligned along the x direction. The cross-section of the duct is elliptical, but it will be supposed that the eccentricity, e, at each cross-section varies with axial location. A crucial assumption in what follows is that the duct varies only slowly along the axis, so a small parameter ε is introduced; later a slow co-ordinate $X = \varepsilon x$ will be used to describe the variation of the geometry along the axis, but for now the eccentricity is

written simply as $e = e(\varepsilon x)$. It will prove particularly convenient to consider a co-ordinate system comprising x together with elliptic co-ordinates in the perpendicular plane; in other words, take Cartesian co-ordinates (x, y, z), with

$$y = e(\varepsilon x)\cosh\rho\cos\theta, \quad z = e(\varepsilon x)\sinh\rho\sin\theta. \tag{1}$$

Here, ρ, θ are analogous to the more usual polar radius and angle in circular polar co-ordinates. If the eccentricity were independent of x then the co-ordinates would simply be standard, *orthogonal* elliptic cylindrical co-ordinates [15, p. 139]. A drawback to this co-ordinate system for general $e(\varepsilon x)$, however, is that it is *non-orthogonal*, and some care will therefore have to be exercised when calculating the various vector differential operators required subsequently. With this in mind, standard methods in differential geometry are followed (see e.g., reference [14]); for a general set of co-ordinates q_1, q_2, q_3, the arc length element ds can be written in the form

$$\mathrm{d}s^2 = \sum_{i=1}^{3}\sum_{j=1}^{3} g_{ij}\,\mathrm{d}q_i\,\mathrm{d}q_j \tag{2}$$

with g_{ij} the metric tensor. In the elliptical co-ordinates take q_1, q_2, $q_3 = \rho$, θ, x, and after some algebra find that

$$g_{ij} = \begin{pmatrix} h_\rho^2 & 0 & \varepsilon g_{13} \\ 0 & h_\rho^2 & \varepsilon g_{23} \\ \varepsilon g_{13} & \varepsilon g_{23} & 1 + \varepsilon^2 \tilde{g}_{33} \end{pmatrix}, \tag{3}$$

where

$$h_\rho = e\sqrt{\sinh^2\rho + \sin^2\theta} \tag{4}$$

is the usual metric element in conventional elliptical co-ordinates (see e.g., reference [5, p. 172]. The terms g_{13}, g_{23}, $\tilde{g}_{33}$ are all $O(1)$ quantities, and need not be stated here since it will be seen that they are not required subsequently.

Expressions will be required for $\nabla\phi$ and $\nabla\cdot\mathbf{U}$ in our non-orthogonal co-ordinate system, where ϕ is the unsteady velocity potential and $\mathbf{U}$ is the steady fluid velocity. The gradient term is straightforward, with

$$\nabla\phi = \frac{1}{\sqrt{g_{11}}}\frac{\partial\phi}{\partial\rho}\,\mathbf{e}_\rho + \frac{1}{\sqrt{g_{22}}}\frac{\partial\phi}{\partial\theta}\,\mathbf{e}_\theta + \frac{1}{\sqrt{g_{33}}}\frac{\partial\phi}{\partial x}\,\mathbf{e}_x, \tag{5}$$

where e_ρ, e_θ, e_x are the unit vectors in the ρ and θ directions (i.e., in the plane transverse to the axis) and in the x (axial) direction respectively. (See reference [14 equation (5.52)], but note that there the vector components are not measured with respect to unit vectors, necessitating the introduction of the factors $1/\sqrt{g_{11}}$, etc., in equation (5).) From equation (3) $\sqrt{g_{11}} = \sqrt{g_{22}} = h_\rho$, and since in subsequent analysis terms of size $O(\varepsilon^2)$ will be disregarded, it follows that g_{33} can be taken to be unity. Hence, the usual formula for $\nabla\phi$ in orthogonal curvilinear co-ordinates [15, p. 148] can be applied to the non-orthogonal system to the asymptotic order required. The formula for the divergence of a vector with components U_1, U_2, U_3 in a non-orthogonal system of co-ordinates q_1, q_2, q_3 is given in equation (6.42) of reference [14], and takes the form

$$\nabla\cdot\mathbf{U} = \frac{1}{\sqrt{\det(g)}}\sum_{i=1}^{3}\frac{\partial}{\partial q_i}\left(\frac{\sqrt{\det(g)}\,U_i}{\sqrt{g_{ii}}}\right). \tag{6}$$

(Note that the result from reference [14] again requires inclusion of factors $1/\sqrt{g_{11}}$, etc., in order to account for unit base vectors, and also requires that the sign of $\det(g)$ to be changed in order to suppress the time-like dimension included in reference [14].) It is easy to show from equation (3) that $\det(g) = h_\rho^4 + O(\varepsilon^2)$, and this means that once again the general result (6) reduces to the standard result for divergence in orthogonal co-ordinates [15, p. 150], to the asymptotic order required, i.e.,

$$\nabla \cdot \mathbf{U} = \frac{1}{h_\rho^2}\left\{\frac{\partial(h_\rho U_\rho)}{\partial \rho} + \frac{\partial(h_\rho U_\theta)}{\partial \theta} + \frac{\partial(h_\rho^2 U_x)}{\partial x}\right\} + O(\varepsilon^2), \tag{7}$$

where U_ρ, U_θ, U_x are components relative to the unit vectors in the ρ, θ, x directions respectively. It must be emphasized, however, that this result is by no means obvious *a priori*, and it is only the slowly varying nature of the duct geometry which has allowed the replacement of the general non-orthogonal results (5) and (6) by the usual expressions in an orthogonal co-ordinate system.

The duct walls will be described by the equations $\rho = \rho_2$ (outer wall) and $\rho = \rho_1$ (inner wall), with of course $\rho_2 > \rho_1$. The assumption of slow geometry variation in the axial direction means that $\rho_{1,2}$ are functions of only the slow variable $X = \varepsilon x$. The limit in which the duct cross-section changes from elliptic to circular along its length will be particularly interesting, and from equation (1) it is clear that this can be achieved by sending $e \to 0$, $\rho \to \infty$; specifically, if the outer duct wall is to become circular with radius R_2 at $X = L$, say, then $e \to 0$ and $\rho_2 \sim \ln(2R_2/e)$ as $X \to L$.

2.2. GOVERNING EQUATIONS

The governing equations to be applied here are identical to those used in reference [8] and are included for completeness. As far as possible the same notation as in reference [8] is used. Lengths are non-dimensionalized by a length-scale of the duct (say axial mean outer radius), R_∞, speeds by a reference sound speed c_∞, and densities by a reference steady density ρ_∞. The steady base flow through the duct satisfies mass conservation,

$$\nabla \cdot (D\mathbf{V}) = 0, \tag{8}$$

where D is the steady density and $\mathbf{V}$ is the steady fluid velocity. A crucial assumption in this analysis is that $\mathbf{V}$ is irrotational, which will allow the vortical and acoustical parts of the unsteady flow to be decoupled. Further, it will be assumed that the steady flow is the isentropic flow of an ideal gas, so that one has Bernoulli's equation

$$\frac{1}{2}|\mathbf{V}|^2 + \frac{C^2}{\gamma - 1} = E, \tag{9}$$

where the steady sound speed C is related to the density by the isentropic relation $C^2 = D^{\gamma - 1}$, γ is the usual adiabatic index and E is a constant.

The unsteady flow through the duct will be assumed to be a small, linear perturbation on top of the steady base flow. Consider single-frequency motion, and write the acoustic potential as $\phi \exp(-\mathrm{i}\omega t)$ (note that this is the opposite sign convention to that of reference [8]). It can then be shown that ϕ satisfies the convected wave equation (see reference [8, equation (4.1a)]

$$\nabla \cdot (D\nabla\phi) - D(-\mathrm{i}\omega + \mathbf{V} \cdot \nabla)\left\{\frac{1}{C^2}(-\mathrm{i}\omega + \mathbf{V} \cdot \nabla)\phi\right\} = 0. \tag{10}$$

Note how the coefficients in this equation depend on the properties of the steady flow, which will in turn depend on spatial (and in particular axial) location.

The boundary conditions to be applied are also the same as in reference [8]. The steady flow will be required to satisfy zero normal velocity on the duct walls, so that

$$\mathbf{V}\cdot\mathbf{n} = 0 \quad \text{on } \rho = \rho_{1,2}. \tag{11}$$

Here, $\mathbf{n}_{1,2}$ are the unit normals to the walls pointing out of the fluid, and are therefore parallel to the vectors $\nabla(\rho - \rho_{1,2}(\varepsilon x))$. By using equation (5) it is easy to see that

$$\mathbf{n}_{1,2} = \mp \frac{h_\rho^{-1}\mathbf{e}_\rho - \varepsilon\rho'_{1,2}\mathbf{e}_x}{(h_\rho^{-2} + \varepsilon^2\rho'^2_{1,2})^{1/2}} + O(\varepsilon^2) \tag{12}$$

with the $\mp$ referring to the inner and outer walls, respectively, and $'$ denoting differentiation with respect to argument. The boundary condition to be satisfied by the unsteady field will depend on the assumed impedance of the walls: if it is supposed that the inner and outer walls are both rigid, then the zero normal-velocity condition $\mathbf{n}\cdot\nabla\phi = 0$ is applicable. With finite wall impedance, the condition formulated by Myers [16] need to be applied—as stated in reference [8] this takes the form

$$-\mathrm{i}\omega(\nabla\phi\cdot\mathbf{n}_{1,2}) = (\mathrm{i}\omega - \mathbf{V}\cdot\nabla + \mathbf{n}_{1,2}\cdot(\mathbf{n}_{1,2}\cdot\nabla\mathbf{V}))\left\{\frac{D}{Z_{1,2}}(-\mathrm{i}\omega + \mathbf{V}\cdot\nabla)\phi\right\} \tag{13}$$

on $\rho = \rho_{1,2}(\varepsilon x)$ respectively. Here $Z_{1,2} = Z_{1,2}(\varepsilon x)$ are the inner and outer wall impedances. This boundary condition has been applied successfully by Rienstra [8] to circular ducts with lined walls. However, for an elliptical duct there turns out to be a fundamental mathematical difficulty, because with finite non-zero $Z_{1,2}$ equation (13) is non-separable in ρ and θ, essentially due to the form of h_ρ. It is only for the rigid-walled case ($Z_{1,2} \to \infty$), and for the practically unimportant pressure-release case ($Z_{1,2} \to 0$), that equation (13) permits a separable solution for ϕ. In what follows only the rigid-wall condition will therefore be considered—inclusion of finite $Z_{1,2}$ would necessitate inclusion of a whole spectrum of coupled modes, which would introduce considerable complexity at this stage. Further work will examine the effects of lining in elliptical ducts.

3. SOLUTION

The solution will be obtained exactly as in reference [8], by the method of multiple scales. The slow axial variable $X = \varepsilon x$ has already been introduced, and $\partial/\partial x$ is thereby replaced by $\partial/\partial x + \varepsilon\ \partial/\partial X$. The geometry parameters (i.e., e, $\rho_{1,2}$) are all functions of X only.

3.1. STEADY FLOW

In reference [8] the steady flow along the slowly varying duct was seen to be governed by one-dimensional gas dynamics, and it is therefore to be expected that the steady solution in the present case will take very much the same form. Write the steady flow as

$$\mathbf{V} = U(X, \rho, \theta)\mathbf{e}_x + V(X, \rho, \theta)\mathbf{e}_\rho + W(X, \rho, \theta)\mathbf{e}_\theta. \tag{14}$$

The cross-sectional mass flux is

$$\int_0^{2\pi}\int_{\rho 1}^{\rho 2} UDh_\rho^2\,\mathrm{d}\rho\ \mathrm{d}\theta \equiv \pi F, \tag{15}$$

where F must be constant. Expansion of the steady flow equations gives, exactly as in reference [8], that

$$U = U_0(X) + O(\varepsilon^2), \qquad C^2 = C_0^2(X) + O(\varepsilon^2), \tag{16, 17}$$

$$D = D_0(X) + O(\varepsilon^2), \qquad V = \varepsilon V_1(X, \theta, \rho) + O(\varepsilon^3), \tag{18, 19}$$

$$W = \varepsilon W_1(X, \theta, \rho) + O(\varepsilon^3), \qquad \frac{U_0^2}{2} + \frac{D_0^{\gamma-1}}{\gamma - 1} = E, \tag{20, 21}$$

while equation (15) now gives

$$D_0 U_0 = \frac{2F}{e^2(\sinh(2\rho_2) - \sinh(2\rho_1))}. \tag{22}$$

Equations (15) and (21) can now be solved for $U_0(X)$ and $D_0(X)$. Note that if one now takes the circular limit ($\rho_{1,2} \to \infty$, $e \to 0$ with $e \exp(\rho_{1,2}) \to 2R_{1,2}$) then Rienstra's equation (3.2) is regained identically. The transverse velocity components V_1 and W_1 must be determined by using the $O(\varepsilon)$ mass condition, together with the $O(\varepsilon^2)$ term in the equation $\nabla \times \mathbf{V} = 0$ and the $O(\varepsilon)$ steady boundary condition. It seems that this can only be completed numerically, but in any event analytical expressions for V_1 and W_1 are not required in subsequent analysis, and one need not pursue this point further.

3.2. UNSTEADY FLOW, LEADING ORDER

To start the unsteady analysis ϕ is written in the standard WKB form used in reference [8], i.e.,

$$\phi(\rho, \theta, x, X) = [A_0(\rho, \theta, X) + \varepsilon A_1(\rho, \theta, X) + \cdots] \exp\left(\frac{\mathrm{i}}{\varepsilon} \int^X \mu(X')\, \mathrm{d}X'\right), \tag{23}$$

where the unknown phase $\mu(X)$ and amplitudes $A_{0,1,\ldots}$ will be determined as part of the solution. Substituting equation (23) into equation (10) and taking $O(1)$ terms yields

$$\mathscr{L} A_0 \equiv \frac{\partial^2 A_0}{\partial \rho^2} + \frac{\partial^2 A_0}{\partial \theta^2} + h_\rho^2 \left[\frac{\Omega^2}{C_0^2} - \mu^2\right] A_0 = 0, \tag{24}$$

where $\Omega = \omega - \mu U_0$. Equation (24) can be solved in terms of Mathieu functions by the method of separation of variables in the transverse co-ordinates.

Upon writing $A_0(\rho, \theta; X) = R(\rho; X)\Theta(\theta; X)$, it is found that

$$R'' + (2q \cosh(2\rho) - a)R = 0,$$

$$\Theta'' + (a - 2q \cos(2\theta))\Theta = 0, \tag{25}$$

where a is a separation constant, primes denote differentiation with respect to the first argument and

$$q = \frac{e^2}{4}\left[\frac{\Omega^2}{C_0^2} - \mu^2\right]. \tag{26}$$

In order to obtain solutions which are periodic in θ, it is well-known [5, chapter 2] that a must take one of a discrete (but infinite) set of values, and that once this has been done two distinct sets of solutions are possible, one set which are even about the ellipse major axis ($\theta = 0$), and another which are odd. In fact, these two general sets of solutions are written as

$$[M_m(X)\mathrm{Ce}_m(\rho, q) + N_m(X)\mathrm{Fe}_m(\rho, q)]\mathrm{ce}_m(\theta, q) \tag{27}$$

and

$$[M_m(X)\mathrm{Se}_m(\rho, q) + N_m(X)\mathrm{Ge}_m(\rho, q)]\mathrm{se}_m(\theta, q), \tag{28}$$

respectively, where $m = 0, 1, \ldots$ labels the value of a chosen to obtain periodicity in θ. The functions $\mathrm{ce}_m(\theta, q)$ and $\mathrm{se}_m(\theta, q)$ are Mathieu functions, and are analogous to $\cos\theta$ and $\sin\theta$, respectively, while $\mathrm{Ce}_m(\rho, q)$ and $\mathrm{Se}_m(\rho, q)$ and $\mathrm{Fe}_m(\rho, q)$ and $\mathrm{Ge}_m(\rho, q)$ are modified Mathieu functions, and are analogous to Bessel functions. The factors $M_m(X)$, $N_m(X)$ are at this stage arbitrary, but their variation in X will be determined from the solvability condition in the next subsection. Given the linearity of the problem, arbitrary linear combinations of modes can be considered by superposition of the results presented here.

The $O(1)$ form of the boundary condition (13) to be applied on $\rho = \rho_{1,2}$ is simply $\partial A_0/\partial\rho = 0$, and substituting equations (27) and (28) into this condition yields the dispersion relation for non-trivial solutions; for the even solution from equation (27)

$$\mathrm{Ce}'_m(\rho_1, q)\mathrm{Fe}'_m(\rho_2, q) = \mathrm{Ce}'_m(\rho_2, q)\mathrm{Fe}'_m(\rho_1, q), \tag{29}$$

while for the odd solutions from equation (28)

$$\mathrm{Se}'_m(\rho_1, q)\mathrm{Ge}'_m(\rho_2, q) = \mathrm{Se}'_m(\rho_2, q)\mathrm{Ge}'_m(\rho_1, q). \tag{30}$$

For given $\rho_{1,2}(X)$ and m, these two transcendental equations are to be solved for q—in fact there will be an infinite discrete spectrum of values of q, which are entirely equivalent to the infinite spectrum of radial modes present for a circular duct. Once possible values of $q(X)$ have been determined, the unknown axial wavenumber $\mu(X)$ can be found by solving equation (26).

Some simplification is possible if a hollow duct is considered by neglecting the terms involving ρ_1; in that case the two solution sets are found by simply taking the first terms in equations (27) and (28), and the dispersion relations (29) and (30) become

$$\mathrm{Ce}'_m(\rho_2, q) = 0 \tag{31}$$

and

$$\mathrm{Se}'_m(\rho_2, q) = 0 \tag{32}$$

respectively

3.3. UNSTEADY FLOW, FIRST ORDER

Now consider terms of size $O(\varepsilon)$ in order to derive a solvability condition for the amplitude A_0. Substituting equation (23) into equation (10) and taking $O(\varepsilon)$ terms yields the expression

$$\begin{aligned} D_0\mathscr{L}A_1 = & -\frac{\mathrm{i}}{A_0}\frac{\partial}{\partial X}\left\{\left[\frac{\Omega U_0}{C_0^2} + \mu\right]h_\rho^2 D_0 A_0^2\right\} - \frac{\mathrm{i}}{A_0}\frac{\partial}{\partial\rho}\left\{\frac{\Omega D_0}{C_0^2}\, V_1 h_\rho A_0^2\right\} \\ & - \frac{\mathrm{i}}{A_0}\frac{\partial}{\partial\theta}\left\{\frac{\Omega D_0}{C_0^2}\, W_1 h_\rho A_0^2\right\}, \end{aligned} \tag{33}$$

where some simplification on the right-hand side has been obtained by using the $O(\varepsilon)$ part of the steady flow continuity equation (8). The $O(\varepsilon)$ terms in the unsteady normal velocity boundary condition yield

$$\frac{\partial A_1}{\partial\rho} = \mathrm{i}h_\rho^2\mu\rho' A_0 \quad \text{on } \rho = \rho_{1,2}. \tag{34}$$

Now proceed as in reference [8] by multiplying equation (33) by A_0 and integrating over $\rho_1 < \rho < \rho_2, 0 < \theta < 2\pi$. After some algebra, and making use of the periodicity of $A_{0,1}$ in θ, the exact result is obtained in the closed form

$$\frac{\mathrm{d}}{\mathrm{d}X}\left\{\left(\frac{\Omega U_0}{C_0^2}+\mu\right)D_0\int_0^{2\pi}\int_{\rho_1}^{\rho_2} h_\rho^2 A_0^2\,\mathrm{d}\rho\,\mathrm{d}\theta\right\}=0, \tag{35}$$

which is the equivalent of the main result in reference [8] (equation 4.10 there). The solution of the problem can now be completed by integrating equation (35) exactly (with constant of integration Q_0^2), and it is found that for the even modes

$$M_m^2(X)=\frac{Q_0^2 C_0^2(X)\mathrm{Fe}_m'^2(\rho_2,q)}{(C_0^2\mu+\Omega U_0)D_0 I}, \tag{36}$$

where

$$I=\int_0^{2\pi}\int_{\rho_1}^{\rho_2}\mathrm{ce}_m^2(\theta,q)\,[\mathrm{Ce}_m(\rho,q)\mathrm{Fe}_m'(\rho_2,q)-\mathrm{Ce}_m'(\rho_2,q)\mathrm{Fe}_m(\rho,q)]^2\,h_\rho^2\,\mathrm{d}\rho\,\mathrm{d}\theta, \tag{37}$$

while $N_m(X)=-M_m(X)\mathrm{Ce}_m'(\rho_2,q)/\mathrm{Fe}_m'(\rho_2,q)$. The integral I can be split into a number of terms, each of which involves an integral in θ multiplied by an integral in ρ. Some of these integrals can be evaluated in closed form by using results from reference [5, p. 177], but no formulae seem to be available for the rest, which must instead be evaluated numerically. In the case of a hollow duct the result simplifies somewhat, with

$$M_m^2(X)=\frac{Q_0^2 C_0^2(X)}{(C_0^2\mu+\Omega U_0)D_0 I} \tag{38}$$

for the even modes (27), where now

$$I=\int_{\rho_1}^{\rho_2}\int_0^{2\pi}\mathrm{Ce}_m^2(\rho,q)\mathrm{ce}_m^2(\theta,q)h_\rho^2\,\mathrm{d}\theta\,\mathrm{d}\rho. \tag{39}$$

Once again, it does not seem possible to write I completely in closed form. For the odd modes, results which are entirely equivalent to equations (36–39) can easily be derived; for instance, for the odd modes in a hollow duct, one can simply replace Ce_m and ce_m by Se_m and se_m in equation (39) respectively.

4. RESULTS

The following representative test case is chosen. Consider first the slowly varying hollow circular duct with radius

$$R_2(X)=1{\cdot}4046-0{\cdot}2592\left(1-\frac{X}{L}\right)^2+0{\cdot}1427\exp\left(-\frac{11X}{L}\right) \tag{40}$$

($0\leqslant X\leqslant L, L=2{\cdot}62$), which is the outer radius of the duct used by Rienstra [8] and is itself based on the CFM56 engine nacelle. The local cross-sections of this intake are now distorted into ellipses, with semi-major and -minor axes $R_y(X)=e(X)\cosh(\rho_2(X))$ and $R_z(X)=e(X)\sinh(\rho_2(X))$, respectively, in such a way that the cross-sectional area is unchanged. This final requirement leads to the relation

$$\sinh(2\rho_2(X))=\frac{2R_2^2(X)}{e^2(X)}. \tag{41}$$

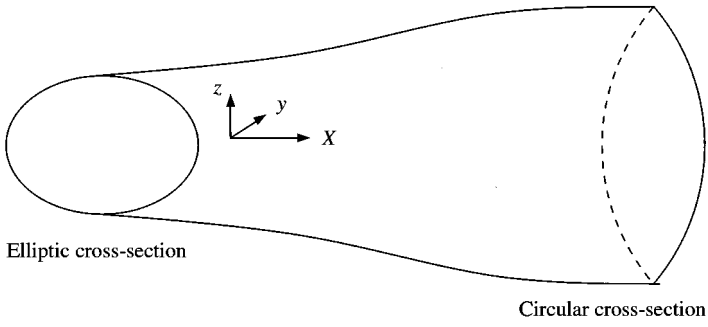

Figure 1. Geometry of the slowly varying elliptic duct.

It is hoped that using an elliptic cross-section with the same area as the original circular cross-section will provide a meaningful appraisal of the effects of non-zero eccentricity. The variation in the eccentricity with axial location is taken to be linear, with $e(0) = 0{\cdot}85$ and $e(L) = 0$, so that the duct cross-section is most elliptic at $X = 0$, and is circular at $X = L$ which can be thought of as the location of the fan (see Figure 1). With $e(X)$ and $R_2(X)$ specified equation (41) can be used to obtain the variation of ρ_2 along the axis. The variations of e, ρ_2 and $R_{z,y}$ with axial location are shown in Figure 2.

The dispersion relations given in equations (31) and (32) were solved to find the values of q for the even and odd modes, respectively, and for m in the range 2–26, as follows. For a given value of q and azimuthal order m, the corresponding value of the separation constant a in equation (25) can be determined by using an eigenvalue solver developed specifically for the Mathieu equation [17], and equations (31) and (32) then solved for q by using Newton iteration. For given q and a the eigenfunction $\mathrm{ce}_m(\theta, q)$, or $\mathrm{se}_m(\theta, q)$, can then be determined by using the power series expansions in section 2.17 of reference [5], while the eigenfunction $\mathrm{Ce}_m(\rho, q)$, or $\mathrm{Se}_m(\rho, q)$, is found either in the same way or (especially close to modal cut-off) by directly integrating the ODE (25a) using initial conditions at $\rho = 0$ specified by the power series in reference [5].

Figure 3 shows the values of q obtained from $m = 2$ and the first radial order (i.e., the lowest value of q from the spectrum of separation constants a in equation 25). It can be seen that, for both odd and even modes, q takes its maximum value at $X = 0$ where the duct is most elliptical, and decays to zero when the duct becomes circular at $x = L$ (the fact that $q \to 0$ as $e \to 0$ can be seen from equation (26)). The differences between the odd and even results were most marked for $m = 2$ where the odd values of q exceed the even ones. For the duct shape given in equation (40) it was found that the values of q for the odd and even modes become coincident when $m > 6$. These results can be compared to the circular duct defined in equation (40) by considering the variation of $2\sqrt{q}/e$, which is analogous to the radial wavenumber for a circular duct. Figure 4 shows that the radial wavenumber of the circular duct lies between the corresponding odd and even results, and all three approach the same value as the duct becomes more circular.

With the values of q determined, the axial wavenumber $\mu(X)$ can be found from equation (26). Here the reduced axial wavenumber, $\sigma(X)$, is calculated which is proportional to the factor $C_0^2\mu + \Omega U_0$ in the denominator of equation (38) and is defined as

$$\sigma(X) = \sqrt{1 - \frac{C_0^2(X)}{\omega^2}[1 - M_x^2(X)]\frac{4q(X)}{e^2(X)}}, \tag{42}$$

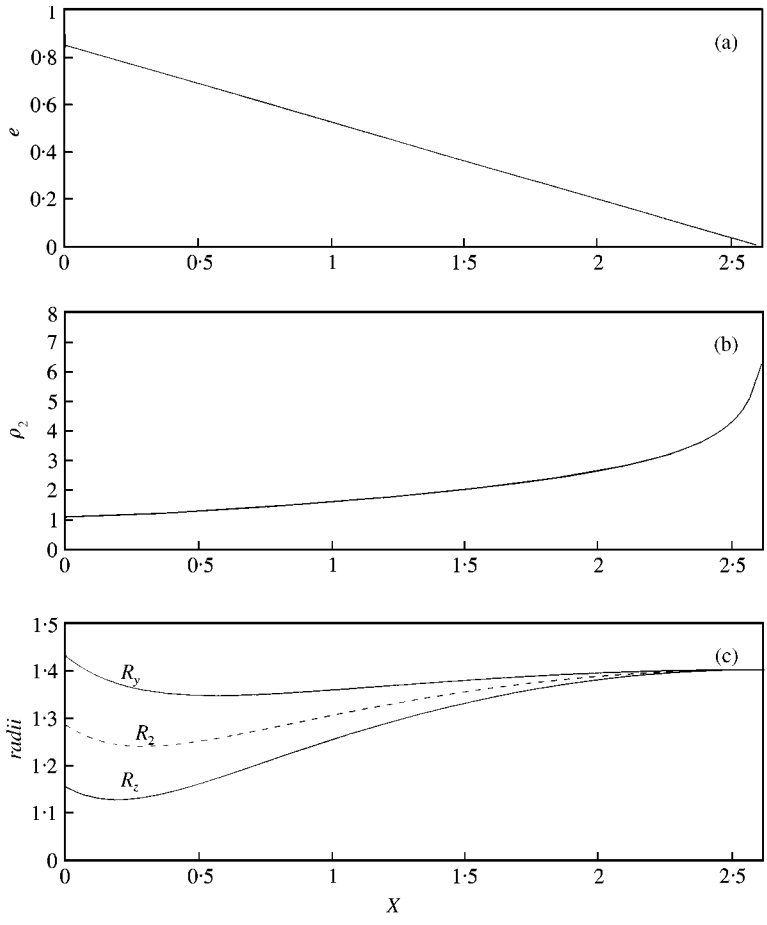

Figure 2. Variation of defining duct parameters with axial location X. (a) Eccentricity e, with $e(0) = 0{\cdot}85$, (b) variation in ρ_2, with $\rho_2 \to \infty$ as $X \to L$. (c) Major (R_y) and minor (R_z) radii of elliptical duct for eccentricity profile given in (a). Also shown is the radius R_2 of the circular duct with the same cross-sectional area at each axial location.

where $M_x = U_0/C_0$ is the steady axial Mach number. When a mode is cut on σ is purely real, and when the mode is cut off σ is purely imaginary.

The variation in σ along the duct, when $m = 2$ and $\omega = 2{\cdot}1$, is given in Figure 5 where comparison is also made with the circular duct (40). It is evident that significant differences in the cut-on/cut-off nature arise between the odd and even modes of the elliptical duct and the circular duct modes. In all cases the slow-variation in the duct cross-section gives rise to a turning point where a mode changes from being cut-on to cut-off. The odd mode gives similar results to the circular duct mode in that it exhibits a single turning point, but the odd mode becomes cut-on slightly further downstream. The even mode, however, produces two turning points and is cut-on at the upstream end of the duct. This general trend is found for other values of m. Both the odd and even modes and the circular duct mode first cut-on at the circular end of the duct (at the same frequency), and as the frequency is increased a single turning point occurs upstream. As the frequency is increased further the modes become cut-on at the upstream end of the duct, giving rise to a second turning point. Eventually, the two turning points coincide and the modes become cut-on along the entire length

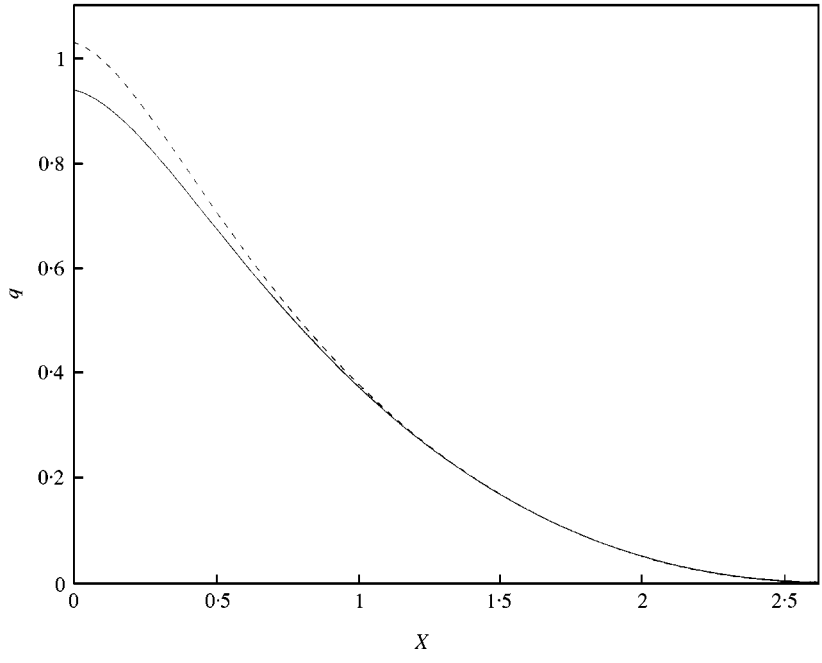

Figure 3. Values of q satisfying the dispersion relation in equation (31) for the even modes (solid line) and equation (32) for the odd modes (dashed line) when $m = 2$.

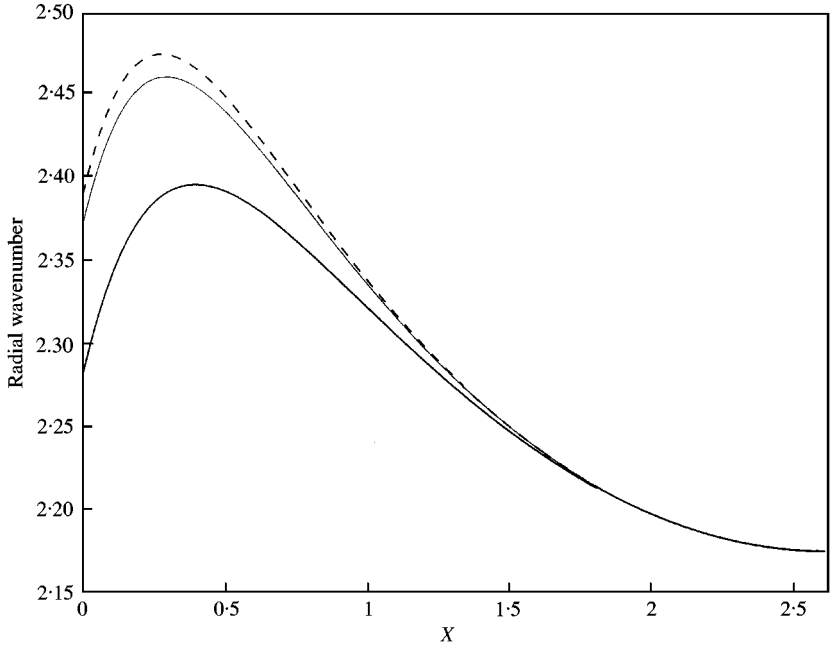

Figure 4. Comparison between radial wavenumber ($m = 2$, first order) for the circular duct (thin solid line) and the corresponding values for the even (thick solid line) and odd (dashed line) modes.

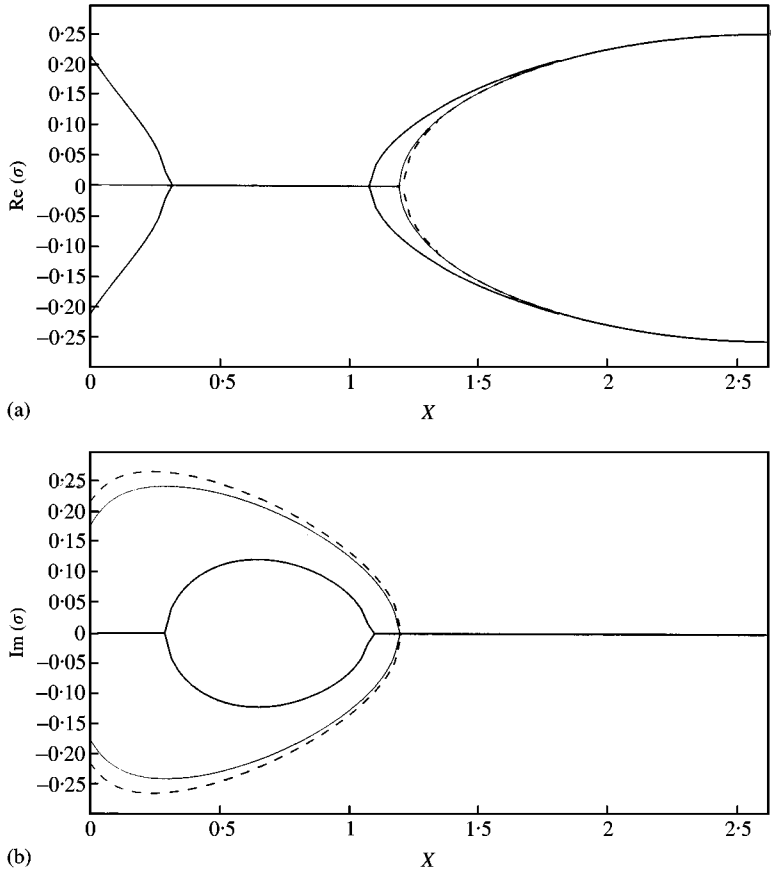

Figure 5. Reduced axial wavenumber σ for $m = 2$, $\omega = 2{\cdot}1$ for first radial order even modes (thick solid lines) and odd modes (dashed lines) of elliptical duct and mode for circular duct (thin solid lines). (a) Re(σ), (b) Im(σ).

of the duct. For mode numbers $m < 6$, as the frequency is increased two turning points first occur for the even modes, followed by the circular duct modes and then finally for the odd modes of the elliptical duct. This can be seen in Figure 6(a) where the frequency ranges for one and two turning points are shown. As m is increased the even and odd modes become equivalent, with complete cut-on all along the duct occurring at lower frequencies than that for the circular duct. Figure 6 shows the frequency ranges for which the different cut-on/cut-off characteristics occur for selected values of m in the range 2–26. For each value of m the frequency ranges are plotted on the same scale, showing that turning points occur over increasingly wider frequency ranges as the value of m gets larger. These frequency ranges coincide for the even and odd modes at larger m, but are different from those of the equivalent circular duct. In summary, for the larger values of m the non-zero eccentricity has the effect of tending to make both the even and the odd modes more cut-on than they would be in the circular duct.

A comparison between modes of different radial order is made in Figure 7 for $m = 2$. Again the frequency ranges for each plot are on the same scale so that, for all mode types, the difference between the frequency at which the mode first cuts on and that where the mode becomes completely cut-on increases with radial order. The trends in the

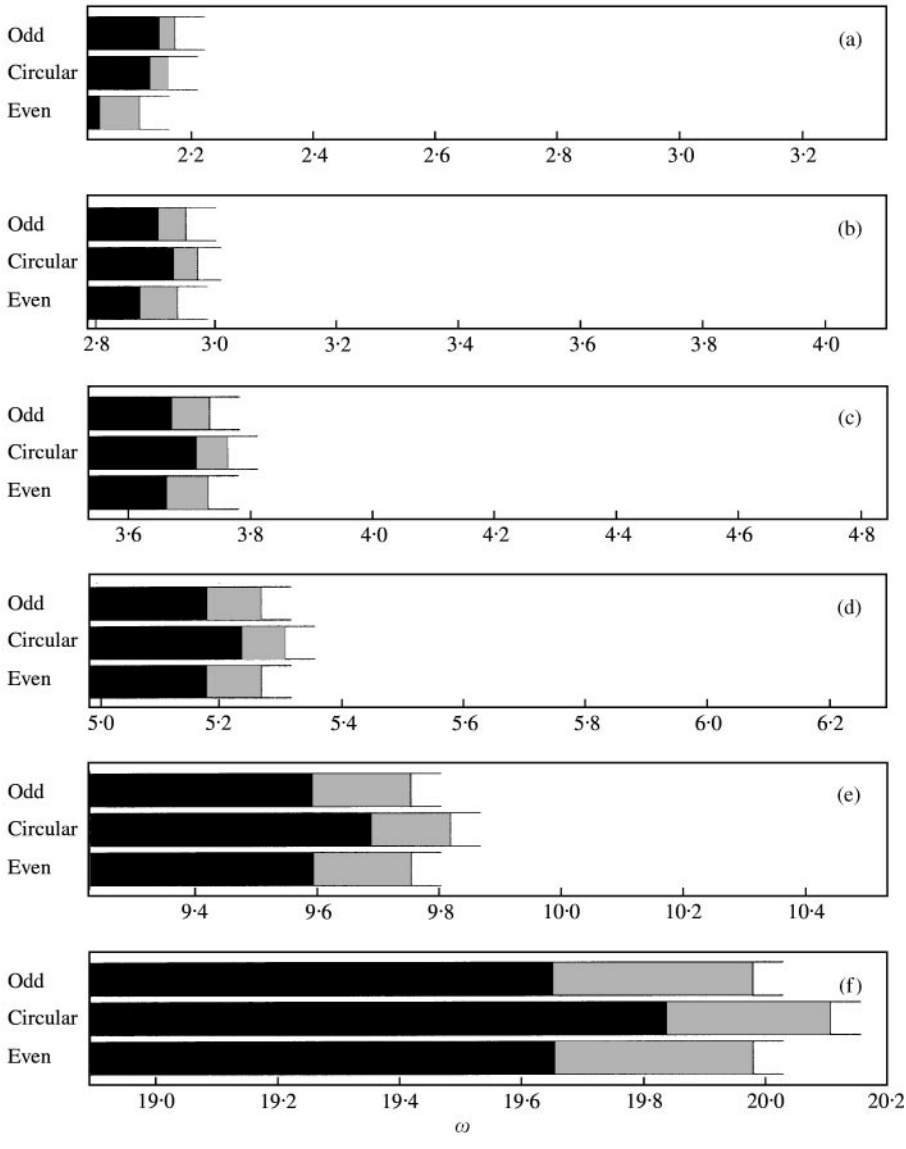

Figure 6. Frequency ranges for which modes (first radial order) exhibit a single turning point (black) and two turning points (grey). Frequencies to the right of the grey regions give rise to modes which are cut-on along the whole length of the duct. (a) $m = 2$, (b) 3, (c) 4, (d) 6, (e) 12 and (f) 26.

cut-on/cut-off behaviour between the odd and even modes and the modes for the circular duct observed for the first radial order are also followed for higher radial orders.

The effect of making the duct more eccentric is shown in Figure 8, where ducts with $e(0) = 0{\cdot}85$ and $1{\cdot}5$ are compared. The increase in eccentricity is found to have a pronounced effect on the even modes, which now first cut-on at the upstream end of the duct but become cut-off further downstream. As a result of this the mode becomes completely cut-on at a much lower frequency when $e(0) = 1{\cdot}5$ compared to when $e(0) = 0{\cdot}85$. The general behaviour of the odd modes remains the same in both cases except that the frequency range for which turning points arise is extended.

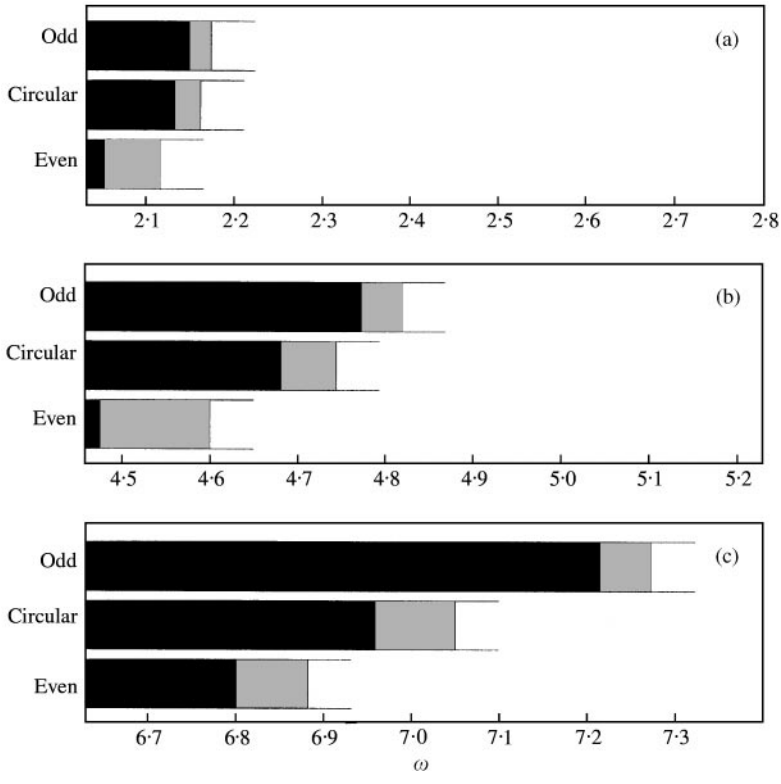

Figure 7. Comparison between modes of different radial order for $m = 2$. (a) First radial order, (b) second radial order, (c) third radial order. Colour coding is the same as in Figure 6.

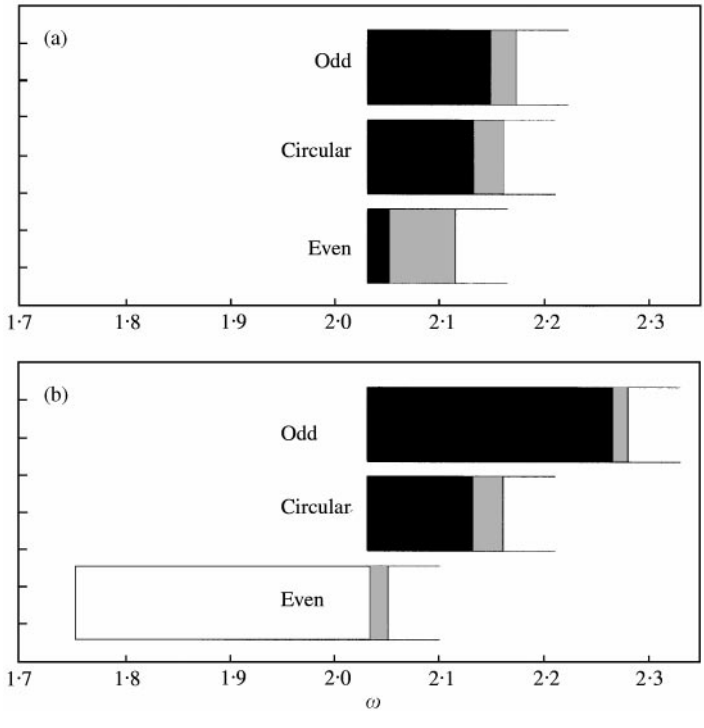

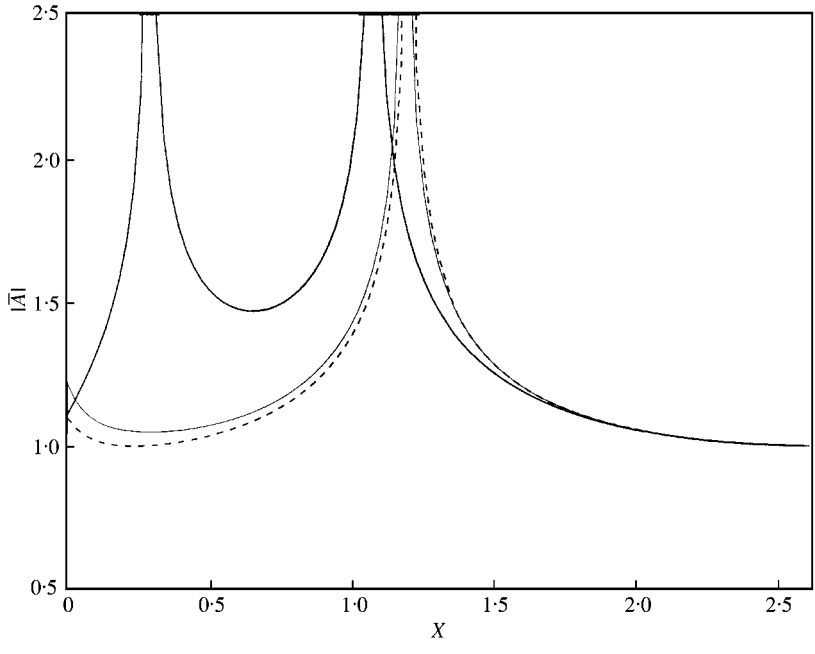

Figure 9. Cross-sectionally averaged amplitudes $\bar{A}$ for $m = 2$, $\omega = 2{\cdot}1$, for the first radial order even mode (thick solid line), odd mode (dashed line) and circular-duct mode (thin solid line).

The cross-sectionally averaged amplitude of the eigenmodes is defined by

$$\bar{A}(X) = \left[\int_0^{2\pi} \int_0^{\rho_2} |A_0(\rho, \theta, X)|^2 h_\rho^2 \, \mathrm{d}\theta \, \mathrm{d}\rho \right]^{1/2}, \tag{43}$$

which, upon using equations (38) and (39), becomes

$$\bar{A}(X) = \frac{Q_0 C_0^{1/2}}{(\omega D_0)^{1/2}} \left| \frac{1}{\sigma^{1/2}} \right|, \tag{44}$$

since $\sigma = [C_0^2 \mu + \Omega U_0]/(\omega C_0)$. This expression breaks down in the vicinity of a turning point, where $\sigma = 0$, and a local analysis must be carried out in order to determine the inner solution in terms of Airy functions. This inner analysis proceeds exactly in the same way as described in reference [18] for the circular duct. One crucial result of the inner analysis is the reflection coefficient of a cut-on wave when it hits the turning point. For a circular duct it is shown in reference [18] that the reflection coefficient is $\exp(\mathrm{i}\pi/2)$, and it is possible to verify that this is also the value for the present elliptical duct. This means that the analysis of mode trapping in a circular duct described in reference [13] could be repeated for an elliptical duct using the theory described in this paper. Figure 9 compares the averaged amplitude for the $m = 2$, $\omega = 2{\cdot}1$ results, normalized to unity at $X = L$. The singular behaviour in this plot indicates the position of the turning points in each case. By forming a composite asymptotic expansion between the outer solution described in this paper and

Figure 8. Comparison of first order radial modes with changing eccentricity for $m = 2$. (a) $e(0) = 0{\cdot}85$, (b) $e(0) = 1{\cdot}5$. Colour coding is the same as in Figure 6 with the white region representing the case of cut-on at the upstream end of the duct, a turning point at some location downstream, and cut-off at the circular end of the duct.

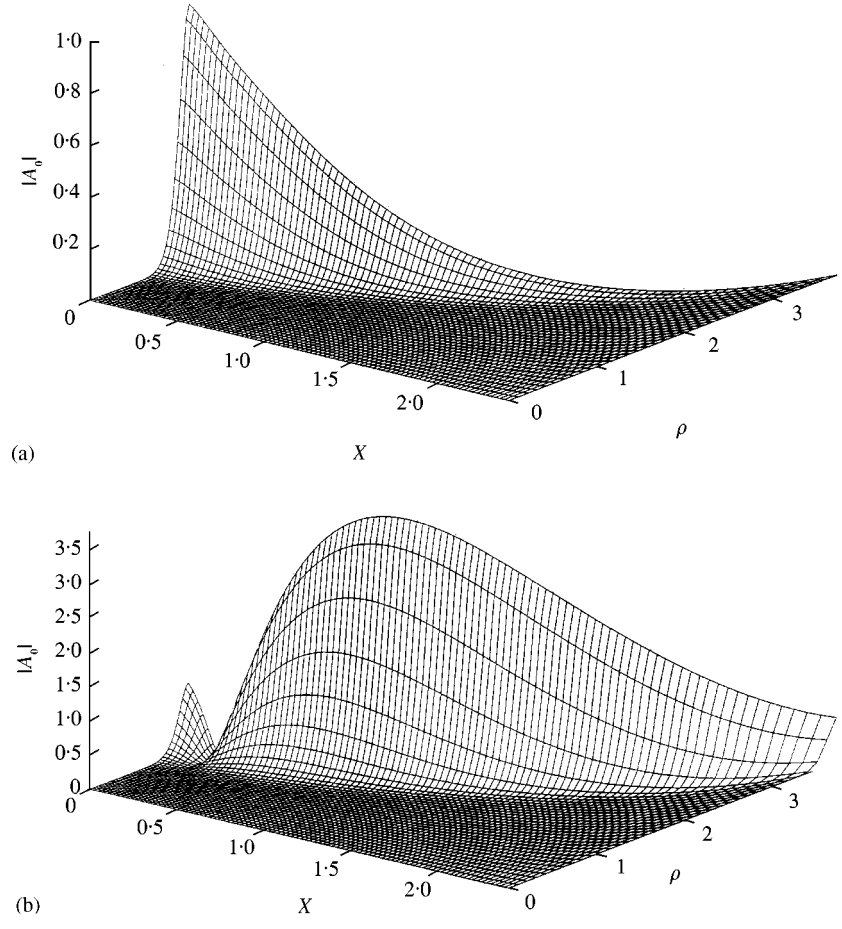

Figure 10. Variation in the modulus of amplitude $A_0(\rho, \theta, X)$ at $\theta = \pi/4$, for $m = 26$, $\omega = 20{\cdot}2$ for the first radial mode. (a) Even-mode amplitude, (b) odd-mode amplitude. Amplitudes are normalized to unity at $X = 0$, $\rho = \rho_2$.

the inner Airy solution a uniformly valid solution which smooths out the singularities seen in Figure 9 could be derived. This composite expansion is given in reference [19] for a circular duct, and the extension to the present elliptical case is straightforward.

The amplitude variation along and across the duct can be determined by using equation (38) with the appropriate form of the integral I. In Figure 10, the variation of $|A_0(\rho, \theta, X)|$ is plotted along the duct at the representative azimuthal location $\theta = \pi/4$. When $m = 26$ it was shown in Figure 6 that the cut-on/cut-off behaviour is the same for the odd and even modes, but Figure 10 shows that the amplitude variations associated with these modes differ substantially. For the frequency used in Figure 10 both the odd and even modes are cut-on all the way along the duct. The modulus of the amplitude for both modes is zero along the centreline $\rho = 0$, and is close to zero over an increasingly wide range of values of ρ as the duct becomes more circular. For a given axial location, both amplitudes have their maximum value on the outer wall. Although the modes are scaled to have unit amplitude at $X = 0$, it is noted that the odd mode is significantly larger as the duct becomes circular, and indeed has passed through higher amplitudes along the duct, than the even mode. In Figure 11, the variation in the cross-sectionally averaged amplitude, $\bar{A}(X)$, is plotted for the same

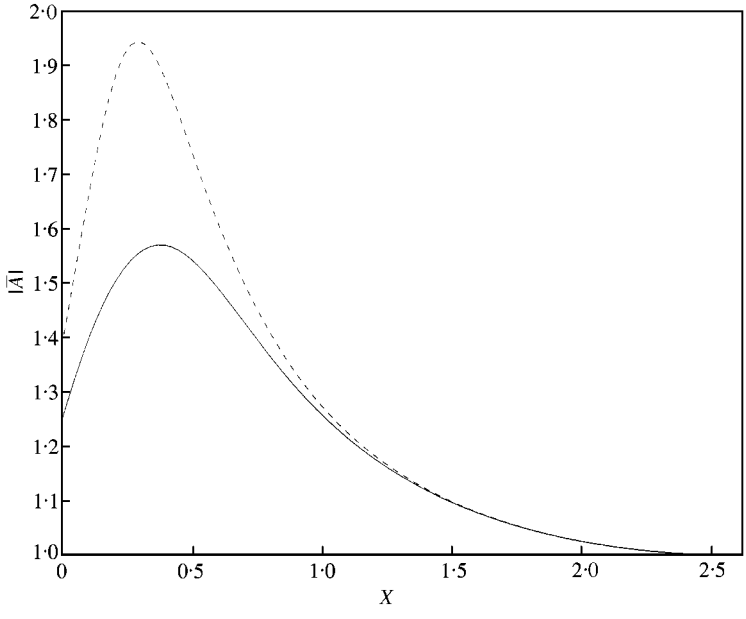

Figure 11. Variation of the cross-sectionally averaged modal amplitude. Conditions as in Figure 10. Circular duct mode (dashed line), even mode (solid line).

case as considered in Figure 10, now with the average amplitudes normalized to unity at the circular end $X = L$. The difference between the behaviour in the elliptic duct and the equivalent circular duct is clear. In the elliptic duct the cross-sectional averages of the odd and even modes are identical for this large value of m, even though, as can be seen in Figure 10, the modal variation with radial coordinate ρ are quite different for a fixed value of θ. It is interesting to note that application of standard circular duct theory would in this case overestimate the averaged modal amplitude all along the duct. A typical methodology for predicting fan farfield noise might well involve predicting the amplitude of a given duct mode launched from the fan once it has reached the nacelle lip, and then use standard diffraction theory for the scattering to the far field. In this case, it follows that the use of circular duct theory would result in a significant error in predicting the energy radiated to the far field.

Finally, one can consider in more detail the azimuthal structure of the elliptical duct modes. In Figures 12 and 13, the modal amplitudes $|\mathrm{Ce}_m(\rho, q)\mathrm{ce}_m(\theta, q)|$ and $|\mathrm{Se}_m(\rho, q)\mathrm{se}_m(\theta, q)|$ are plotted for $m = 2$ and 26 respectively. For low values of m these mode shapes are relatively flat, with just narrow localized regions of small amplitude. However, for larger m the modes only have significant amplitude towards the outside of the duct, and have relatively small amplitude for smaller ρ. The azimuthal distribution of the modes is determined by the values of m, with the number of lobes in these modulus plots being $2m$. In short, the structure of the elliptical duct modes is similar to that of standard circular duct modes, but of course fitted to the elliptical geometry. A very attractive way of describing the structure of the modes in a circular duct is provided by high-frequency asymptotics and ray theory, as in reference [20]. This approach is rather different to the one adopted in this paper, but the ray theory could in principle be applied to our present duct as well (see for instance reference [21]). One difficulty with following the approach described in reference [20] might be the fact that large-argument/large-order asymptotic expansions of the

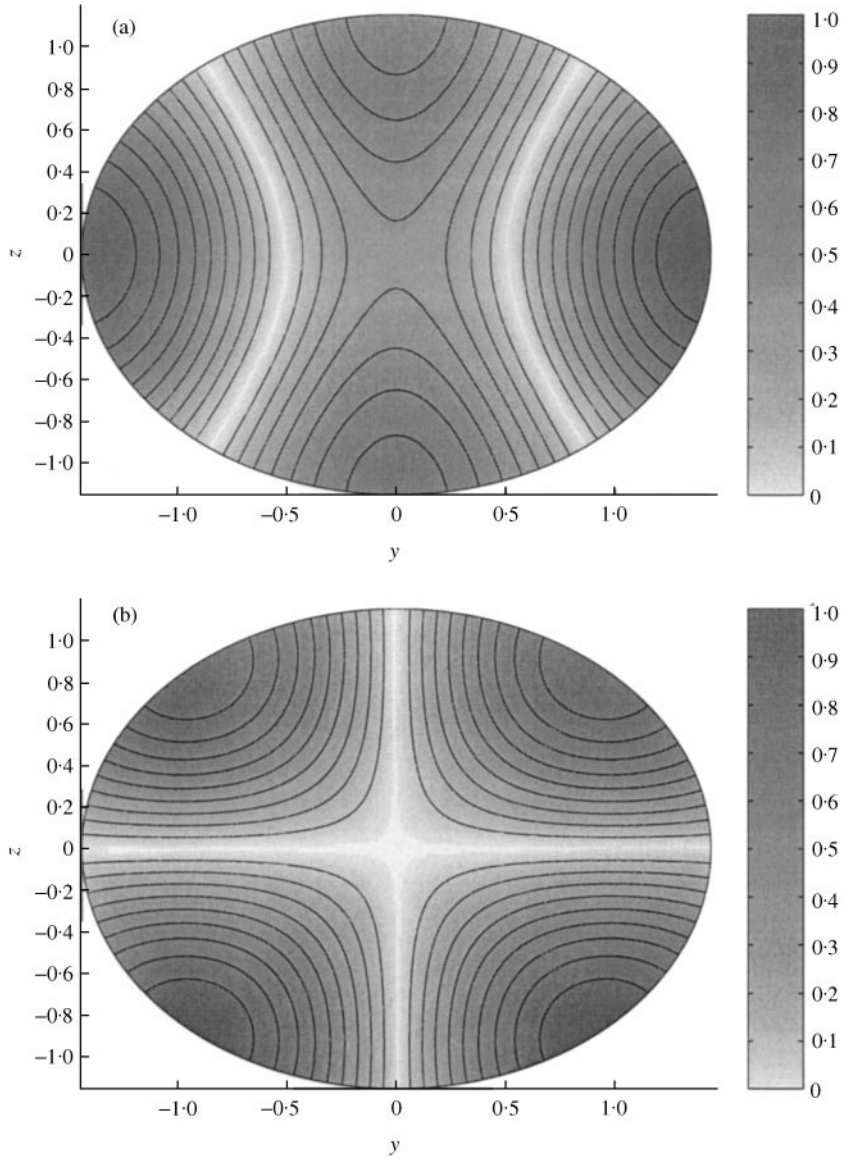

Figure 12. Cross-sectional variation of (a) $|\mathrm{Ce}_m(\rho, q)\mathrm{ce}_m(\theta, q)|$ and (b) $|\mathrm{Se}_m(\rho, q)\mathrm{se}_m(\theta, q)|$ for $m = 2$. Plots made at $X = 0$, other conditions as in Figure 9.

Mathieu function, analogous to the Debye expansion of the Bessel function, do not seem to be so readily available.

5. CONCLUDING REMARKS

In this paper, it has been demonstrated that the propagation of acoustic modes in a realistic aeroengine duct is strongly affected by the local cross-sectional shape of the duct. Moreover, these effects are significant over the whole range of practical azimuthal orders, from the low order modes relevant to the dynamic response of the fan right up to the high

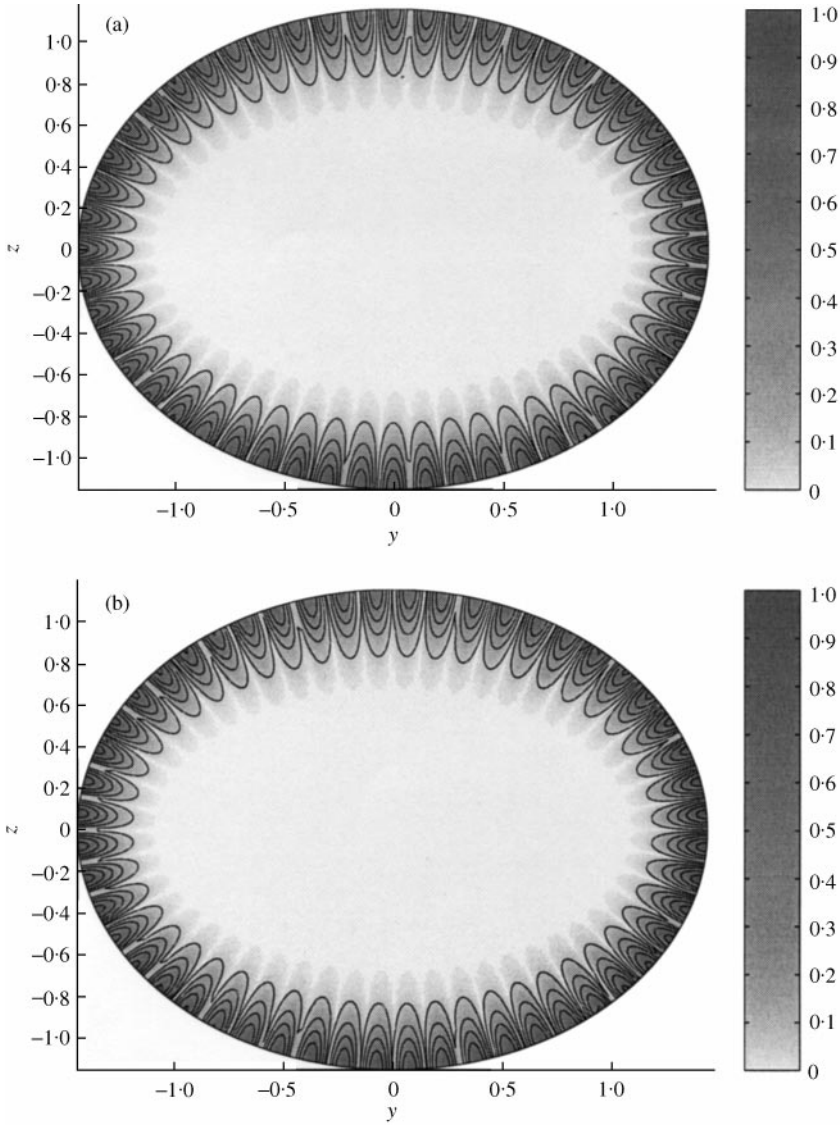

Figure 13. As in Figure 12, but now with $m = 26$ and other conditions as in Figure 10.

order modes associated with the farfield radiation. It is also particularly noteworthy that the behaviours of the odd and even modes in the elliptic duct are quite different; even for the higher azimuthal orders, while the cut-on properties and cross-sectionally averaged amplitudes are almost identical, the radial variations of the even and odd modes are very different (see Figure 10). One trend which is clearly apparent from the results is that the non-zero eccentricity of the duct causes the even elliptic modes to become more cut-on than they would have been in the equivalent circular duct. This could be of some practical concern if one were in a situation in which a given mode was only just cut-off, and would therefore not radiate to the far field, according to standard circular-duct theory, since the asymmetry in the real nacelle could then cause it to be cut-on, with a corresponding increase in farfield noise.

Two extensions of the current analysis are needed for full practical application. One involves the consideration of more general cross-sectional shapes, still with slow axial variation. This would presumably require numerical determination of the axial eigenvalue spectrum at each axial location, but it may well still be possible to determine the amplitude variation along the duct in the way described here. A second extension involves the inclusion of acoustic liners. It has already been noted that the wall normal velocity boundary condition is non-separable, so that a given mode could be scattered into modes of other radial and circumferential orders. Also, inclusion of the liner would introduce complex axial wavenumbers and hence Mathieu functions of complex argument, which appear to have received little attention in the literature. Work in these directions will continue.

ACKNOWLEDGMENTS

AJC acknowledges financial support from EPSRC under grant reference GR L80317. The authors are very grateful to Dr Hubert Meitz of DAMTP for making available his code for calculating Mathieu functions, and for helpful discussions.

REFERENCES

1. A. D. PIERCE 1989 *Acoustics*. New York. Acoustical Society of America.
2. D. G. CRIGHTON 1973 *Journal of Fluid Mechanics* **59**, 665–672. Instability of an elliptic jet.
3. P. J. MORRIS 1988 *American Institute of Aeronautics and Astronautics Journal* **26**, 172–184. Instability of elliptic jets.
4. P. J. MORRIS 1995 *Physics of Fluids* **7**, 185–194. The spatial stability of compressible elliptic jets.
5. N. W. MCLACHLAN 1964 *Theory and Application of Mathieu Functions*. New York: Dover.
6. A. H. NAYFEH and D. P. TELIONIS 1973 *Journal of the Acoustical Society of America* **54**, 1654–1661. Acoustic propagation in ducts with varying cross section.
7. A. H. NAYFEH, B. S. SHAKER and J. E. KAISER 1980 *American Institute of Aeronautics and Astronautics Journal* **18**, 515–525. Transmission of sound through nonuniform circular ducts with compressible mean flows.
8. S. W. RIENSTRA 1999 *Journal of Fluid Mechanics* **380**, 279–296. Sound transmission through lined ducts with flow.
9. C. M. BENDER and S. A. ORSZAG 1978 *Advanced Mathematical Methods for Scientists and Engineers*. New York: McGraw-Hill.
10. S. W. RIENSTRA and W. EVERSMAN 1999 *American Institute of Aeronautics and Astronautics Journal Paper* 99-1821. A numerical comparison between multiple-scales and FEM solution for sound propagation in lined flow ducts.
11. H. LEVINE and J. SCHWINGER 1948 *Physics Reviews* **73**, 383–406. On the radiation of sound from an unflanged circular pipe.
12. G. HOMICZ and J. A. LORDI 1975 *Journal of Sound and Vibration* **41**, 283–290. A note on the radiative directivity pattern of duct acoustic modes.
13. A. J. COOPER and N. PEAKE 2000 *Journal of Fluid Mechanics* **419**, 151–175. Trapped acoustic modes ion aeroengine intakes with swirling flow.
14. B. F. SCHULTZ 1985 *A First Course in General Relativity*. Cambridge: Cambridge University Press.
15. M. R. SPIEGEL 1959 *Theory and Problems of Vector Analysis*. New York: Schaum.
16. M. K. MYERS 1980 *Journal of Sound and Vibration* **71**, 429–434. On the acoustic boundary condition in the presence of flow.
17. R. B. SHIRTS 1990 Idaho National Engineering Laboratory. Code available at http://www.netlib.org/toms/721.
18. S. W. RIENSTRA and A. HIRSCHBERG 1999 *An Introduction to Acoustics*. Report IWDE 99-02. Technische Universitet Eindhoven.

19. M. H. HOLMES 1995 *Introduction to Perturbation Methods*. Berlin: Springer-Verlag.
20. C. J. CHAPMAN 1999 *Journal of Fluid Mechanics* **281**, 293–311. Sound radiation from a cylindrical duct. Part 1. Ray structure of the duct and of the external field.
21. L. A. WEINSTEIN 1969 *Open Resonators and Waveguides*. Boulder, Colorado Golem Press.